PART II

STEAM REFORMING OF n-HEXANE ON PELLET AND MONOLITHIC CATALYST BEDS

A Comparative Study on Improvements due to Heat Transfer

INTRODUCTION

Steam reforming of desulfurized heavy hydrocarbon fuels for fuel cell applications of interest to electric utilities requires high catalyst temperatures (1500-1700°F) and high steam-to-carbon ratios. Since steam reforming is endothermic, the heat must be transferred through the reactor walls and throughout the catalyst bed. The temperature required on the outside walls of the reactor, therefore, is in excess of the temperature within the catalyst bed. Preheat of the fuel and steam prior to entry into the catalyst bed can provide a certain amount of the energy required, but is limited to the point at which steam-cracking of the fuel (which can produce soot) occurs. Most of the reaction energy required, therefore, is supplied through the reactor walls. Steam reforming of heavier fuels, which normally contain as much as 0.3-0.5 wt.% sulfur, without removing the sulfur, would require even higher wall temperatures than for clean fuels to inhibit the poisoning of base metal catalysts. However, as higher temperatures are reached, the reactor materials become more expensive and less durable. In addition, the high temperature operation is less efficient because of the higher heat loss in the exhaust gas. Thermal gradients through the catalyst bed from wall to centerline contribute to sintering or poisoning of the catalyst, particularly during a load-following transient that might be anticipated in actual fuel cell use in utilities.

Honeycomb monolithic supports for steam reforming catalysts appear promising in that they have the potential of improving radial heat transfer necessary to reduce thermal gradients in the catalyst bed. The connecting walls of the monolith provide a continuum for superior heat transfer relative to the poor heat transfer through edge and point contact present in a pellet bed. With the more uniform bed temperature of a monolith, the possibility of hot spots and areas of nonreactive holes due to poor packing can be eliminated. The more uniform temperature also results in a more uniform reaction zone that is easier to control. This is of particular importance in avoiding soot formation in the catalyst bed. Another important factor is that because of better heat transfer properties, monoliths are expected to "respond" faster during transients in fuel cell load following. As a result of better heat transfer through the catalyst bed, less expensive wall material with longer lifetime can be implemented. Successful application of monolithic catalysts to steam reformers could thus offer substantial energy savings in both steady state and transient operation.

We have recently reported (11) on steam reforming tests of n-hexane on monolithic catalyst beds. A 20-inch long bed was loaded first with a commercial pellet steam reforming catalyst (G-90C), and then with two different honeycomb monoliths. In one case, the total length of the bed was made up of ceramic monoliths (Cordierite) supporting nickel catalyst, while in a second case, a hybrid configuration was used having 8 inches of a metal monolith support (Kanthal), also impregnated with nickel, followed by 12 inches of the same ceramic monolith catalyst as in the first case. A washcoat of γ-alumina was used on both types of monoliths to provide a high surface area for the nickel catalyst.

Comparative tests between the pellet and monolithic beds were run at similar operating conditions (steam-to-carbon ratios, external heat flux, inlet temperatures and space velocities). Results from tests with the ceramic monolith have shown that the Cordierite support with its γ-alumina washcoat was not stable when used throughout the length of the bed; a rapid disintegration of the solid was observed at conditions common to steam reformers. This instability was probably due to breaking of the washcoat (through phase changes and carbon formation), and subsequent extraction of the support silica by steam at the high temperatures of operation.

In following tests, the combination of a metal honeycomb monolith (at the top of the bed) and a ceramic monolith (at the bottom) was tested in the steam reformer. With this configuration, the shortcomings of using the Cordierite monolith exclusively throughout the total length of the bed were expected to be alleviated because the metal monolith at the top would have better heat transfer characteristics and, thus, be less prone to carbon formation. The Cordierite monolith at the end of the bed would complete the steam reforming reaction with lower probability of hydrothermal disintegration due to lower amounts of steam present there. This "hybrid" monolith was found to have better radial heat transfer properties than the pellets, and a similar conversion efficiency to that of the pellets, initially. In later tests, however, which followed carbon formation in the bed (and irreversible plugging of many monolith cells), the conversion characteristics of the hybrid monolith were changed. Intermediate hydrocarbons (ethylene, propylene) were produced in higher amounts, and temperatures dropped because of higher effective flowrates through unplugged cells. Carbon formation in the Cordierite monolith followed by long desooting periods caused the complete physical breakdown of portions of

this monolith. The metal monolith pieces, however, were retrieved in good condition, even though many of their cells had been plugged with carbon.

In the work reported here, we have used only metal monolithic supports, which appear to have better radial heat transfer characteristics in the steam reformer than conventional pellet beds, and which were also found to be stable in our previous tests. Reaction temperatures and products, and the propensity for carbon formation have been compared between a commercial catalyst pellet (G-90C) bed and two different metal monolithic catalysts under similar operating conditions.

EXPERIMENTAL

Apparatus

The steam reforming system used in this work is simply a tubular packed bed reactor positioned inside a three-zoned furnace. Figure 20 shows a schematic of this steam reforming system. Fuel is vaporized in an electrical heater and mixed with steam that is also vaporized and preheated by electric heaters. The hot mixture is then fed down through the catalyst bed.

A 2.5 inch I.D. by 31.5 inch long Inconel reactor was used in all tests. Both end pieces are constructed with two multiport accesses for thermocouple inlets to the catalyst bed. The reactor is mounted vertically inside a hinged type 35 kW Mellen furnace. Three-zone heating is provided by three individually controlled zones in the furnace. The furnace is 29.5 inches long but the design of the furnace is such that the top 2 inches and the bottom 2.5 inches are unheated and contain insulating material. Thus, approximately the top 4 inches of the reactor are at lower temperature than the main body of the furnace. For this reason, this area is not filled with catalyst. In this phase of the work, the inlet to the reactor was made of refractory material with a conical shape to avoid stagnation areas and to provide uniform inlet conditions. Pieces of multi-channel alumina sponge were used to fill the reactor inlet. All feed lines, heaters, etc., were insulated to minimize heat losses.

Bed temperatures were monitored by Inconel sheathed chromel-alumel thermocouples. In the tests described here the catalyst bed was 8 inches long, so only sixteen thermocouple ports in the top flange were used. Figure 21 shows a schematic of the catalyst bed and the position of the imbedded thermocouples.

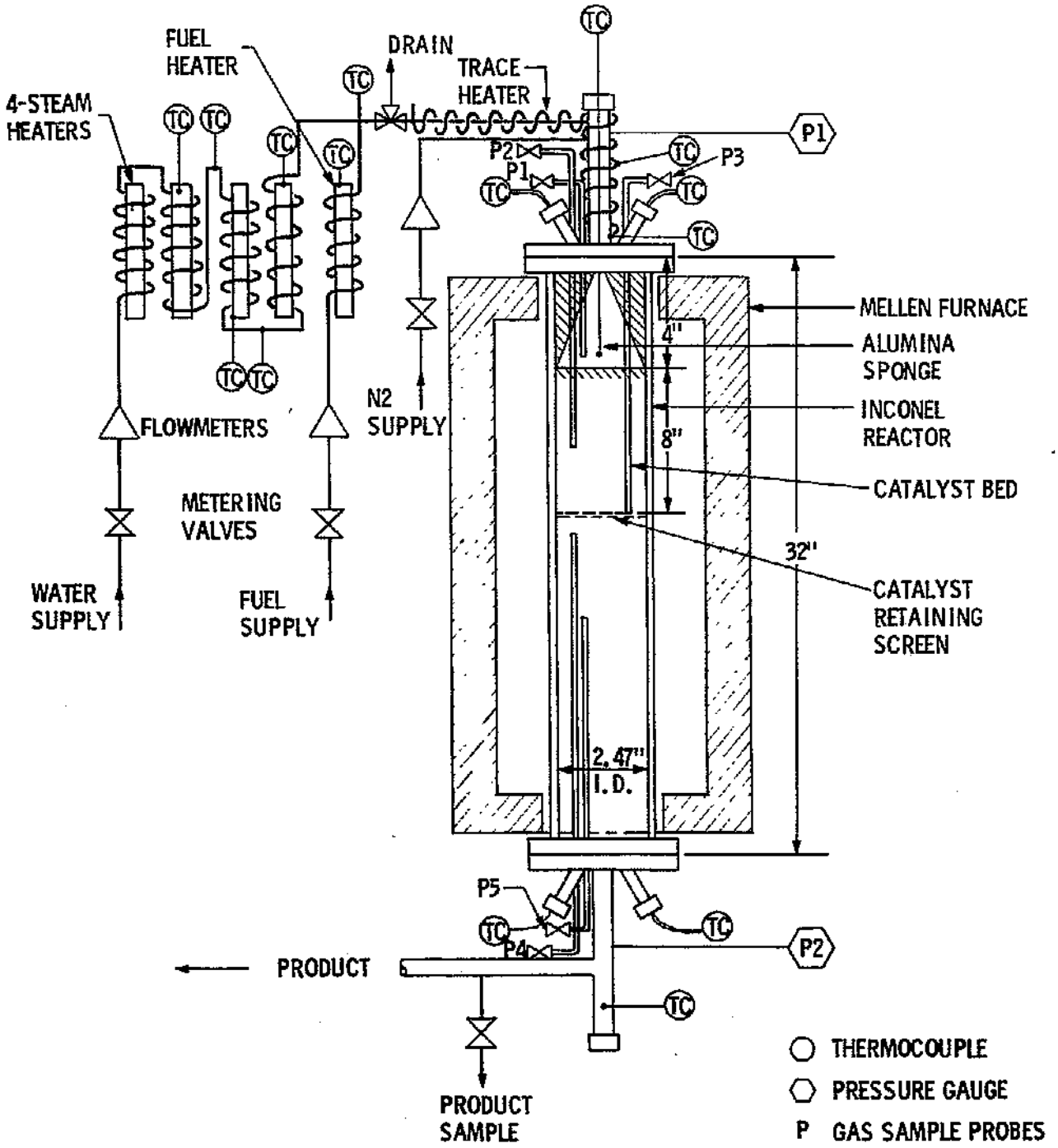

Figure 20. Schematic of the Steam Reforming System.

Additional thermocouples were used externally to monitor the reactor wall temperatures. Three gas probes (1/8 inch I.D.) were also installed through the top flange to sample gases from different bed locations. Gas samples were continuously analyzed for hydrogen, carbon monoxide, carbon dioxide and total hydrocarbons with analyzers specific for each gas. A HP-5830 gas chromatograph (FID) was also used for individual hydrocarbons identification and analyses.

Materials

(a) Fuel

n-Hexane was the choice of hydrocarbon for steam reforming, in part because whatever is unconverted can be measured by the gas chromatograph. Technical grade was used for economy reasons. The chemical composition of the technical grade n-hexane purchased from Phillips Petroleum is as follows:

Normal Hexane:	97.7% (Min = 95.0%)
Methylcyclopentane:	2.1%
3-methylpentane:	0.2%
2-methylpentane:	trace

(b) Catalysts

Steam reforming tests in this phase of the work were performed on catalysts supported by metal monolith and ceramic pellets. The monolithic bed used was comprised of four, 2-inch long pieces, as shown in Figure 21. These had a honeycomb geometry (hexagonal channels) with a cell density of 250 cells/in^2. The monolithic catalyst substrate was made

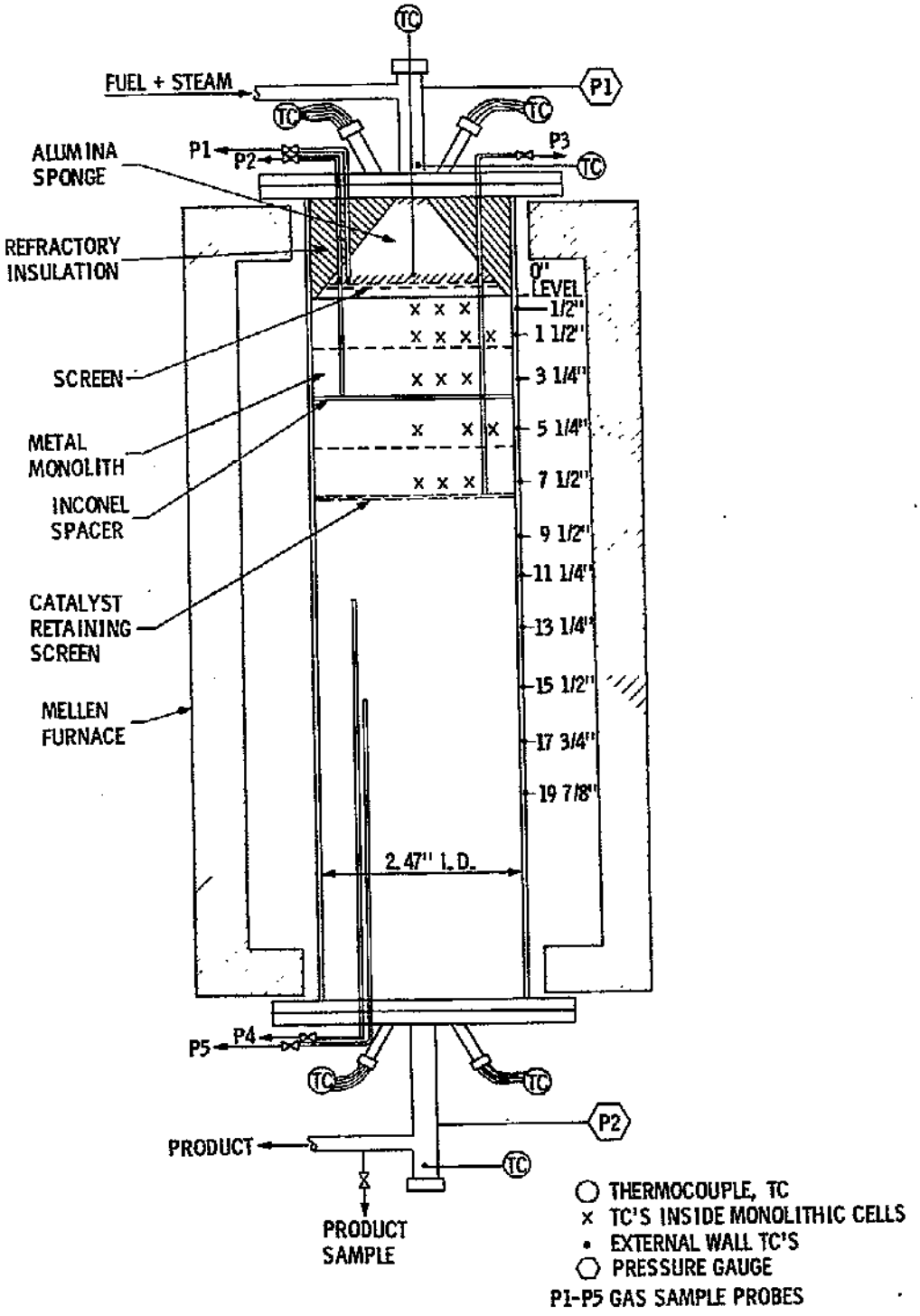

Figure 21. Schematic of the Steam Reformer. Locations of the thermocouples and gas sampling probes are indicated for the honeycomb metal monolith.

from Kanthal (Fe-Cr-Al alloy) which was washcoated with γ-alumina, then impregnated with nickel. The first metal monolith (I) used was the same as the one used in earlier tests (11) in series with the ceramic (Cordierite) monolith. The composition of the four monolithic pieces as received is shown in Table VIII.

Following the series of tests on metal monolith I, new steam reforming tests were run using a conventional pellet catalyst. The commercial Girdler G-90C catalyst was used in the form of cylindrical tablets (1/4 in x 1/4 in). This is composed of nickel impregnated on a ceramic support (calcium aluminate). The physical and chemical characteristics of this catalyst are given in Table VIII.

Upon completion of the tests with the pellet catalyst bed, a new metal supported monolithic catalyst (II) was tested in the steam reformer. The same substrate was used as before (Kanthal), washcoated with γ-alumina, but its impregnation with nickel catalyst was done in-house. After the four monolithic segments had been cut to fit tightly inside the reactor tube, they were impregnated with nickel. The final composition of each segment of the metal monolith II is shown in Table VIII.

TABLE VIII

PHYSICAL AND CHEMICAL CHARACTERISTICS OF STEAM REFORMING TEST CATALYSTS

A. METAL MONOLITH I (4 pieces, 2 inches long each), as purchased:

250 cells/in^2 Kanthal support/γ-Al_2O_3 washcoat/NiO catalyst

Weight, g (before cutting)	#1	#2	#3	#4
Bare Metal (Kanthal)	177.4	171.8	171.9	172.4
γ-Al_2O_3 washcoat	9.76	10.31	9.63	10.50
NiO	6.21	5.33	5.33	5.69
γ-Al_2O_3/Kanthal, %	5.50	6.00	5.60	6.09
NiO/Al_2O_3, %	63.63	51.70	55.35	54.19

B. GIRDLER G-90C (1/4" x 1/4" cylindrical tables), 8-inch long bed

Chemical Analysis, Wt. %

NiO	19.2
γ-Al_2O_3	78.6
CaO	2.0
SiO_2	0.2

C. METAL MONOLITH II (4 pieces, 2 inches long each) impregnated in-house

250 cells/in Kanthal support/γ-Al_2O_3 washcoat/NiO catalyst

Weight, g (after cutting)	#1	#2	#3	#4
Bare metal (Kanthal)	123.08	131.95	137.47	129.33
γ-Al_2O_3 washcoat	8.24	7.92	7.83	8.53
NiO	7.08	6.38	6.20	5.97
γ-Al_2O_3/Kanthal, %	6.69	6.00	5.70	6.60
NiO/Al O , %	85.92	80.56	79.18	69.99

Procedure

For start-up of the steam reforming system, each zone of the Mellen furnace was heated to a specified temperature so that a uniform temperature would be reached along the outside reactor wall. Hydrogen was introduced into the reactor and the nitrogen flow, used as inert protection, was shut off. The hydrogen flow was maintained during this heating period to reduce the nickel catalyst. The steam heaters were turned on, and a specified water flow was heated and dumped before entering the reactor as shown in Figure 20. When the temperature of the steam coming out of the last steam heater was 1200°F, the steam was diverted into the heated reactor. After the reactor inlet temperature reached 1000°F, the trace heater at the reactor inlet, and the fuel heater were turned on. Heated fuel was gradually added to the steam, until the specified flow was reached. The fuel temperature was maintained between 400°F and 550°F. The steam heaters were adjusted to maintain the reactor inlet at 1000°F.

During each test, reactant flowrates, product compositions, catalyst bed temperatures, and bed pressure drop were monitored. In all tests, after steady state was established, temperatures were recorded and gas samples from the reactor exit as well as from each of the bed locations shown in Figure 21 were analyzed. Dry volume percentages of H_2, CO, CO_2 and total hydrocarbons were calculated from gas analyzer data. The detailed volume percentages and analyses of hydrocarbons were calculated from G.C. (FID) data.

A pressure rise during a run was an indication that solid carbon was forming. In addition, carbon fines were sometimes detected in the probe condenser or in the exhaust filter. To desoot the bed, the reactor inlet temperature was

raised to 1200°F, and the steam flowrate was increased while the fuel was turned down to around 0.5 lb/hr, resulting in a $(S/C)_m$ ratio of about 5. The system was left at these conditions until the CO_2 and H_2 levels in the exhaust were stabilized, and the pressure drop through the bed was less than 5 psig for approximately 1 hour. Following desooting, new test parameters were set for continued operation. At the end of operation, the system was shut down under nitrogen with steam shut-off being preceded by the fuel.

RESULTS AND DISCUSSION

(A) Tests With The Metal Monolith I

Initially, steam reforming tests were performed on the metal monolith catalyst I that had been used in the hybrid monolith experiments (in series with the ceramic monolith segments). The composition of the monoliths used are shown in Table VIII.

Tests SR-208 through 226 were run with n-hexane using this 8-inch long metal monolith bed at P = 1 atm, T_{inlet} = 1000°F, and for $(S/C)_m$ ratios of 2.5, 3.0 and 3.5. External reactor wall temperatures of 1500°F and 1700°F were used with nominal reactants' space velocities equal to 2000 and 4000 hr^{-1}. The nominal space velocity is defined here by:

$$S.V. = \frac{[\text{Vol. Flowrate of Reactants, } ft^3/hr]_{\ 60°F,\ 14.7\ psia}}{\text{Reactor Volume, } ft^3}$$

The reactor volume rather than the monolithic catalyst volume is used in this expression. In all tests, the bed temperatures, product yields, and carbon-forming tendency were examined and compared with data from previous tests in which the 20-inch long hybrid monolith or pellet bed were used. The data from these tests are summarized in Table IX. In order to keep nominal space velocities the same as with the longer beds used in earlier tests (2.5 times longer), the flowrates (and, hence, the flow velocities) used in the present study were 2.5 times lower.

In Figures 22 and 23, the dry gas volume percentages of the various gaseous species are plotted as a function of the catalyst bed length for the short metal monolith, and the longer hybrid monolith and pellet bed. Higher amounts of total hydrocarbons and lower amounts of hydrogen and carbon monoxide were found at the level of probe 3 when the short metal monolith was used than for the other two catalyst beds. The amount of unconverted hexane at this level was lower with the metal monolith, while higher amounts of intermediates (ethylene, propylene, etc.) and methane were produced in this case. This finding indicates that cracking reactions in the gas phase rather than steam reforming on the catalyst surface were taking place throughout the length of the monolith cells under these conditions. Since the conversion of the fuel at the exit of the 8-inch long monolith is lower than that at the corresponding point of the longer monolith or the pellet bed (location of gas probe 3), this means that external mass transfer limitation exists (diffusion of the reacting species from the gas phase to the catalyst surface). All operating conditions examined here were found to be mass transfer limited.

TABLE IX

STEAM REFORMING OF N-HEXANE ON THE METAL MONOLITH I

TEST	$(S/C)_m$	(1) $\dot{m}_w$	(1) $\dot{m}_f$	(2) SPACE VELOCITY	(3) T_{WALL}	CARBON	(4) GAS PROBE	DRY GAS COMPOSITION, MOL %											
		LB/HR	LB/HR	HR^{-1}	°F		AT INCHES	H_2	CO_2	CO	HC_T	CH_4	C_2H_4	C_2H_6	C_3H_6	C_3H_8	C_4	C_5	C_6H_{14}
208	3.0	2.0	0.53	2000	1500	NO	EXIT	62.77	15.61	12.60	9.28	3.60	3.27	0.77	0.81	0.01	0.19	0.05	0.58
209	3.0	2.0	0.53	2000	1500	NO	4-1/8	59.93	15.67	11.62	13.01	2.34	1.88	0.47	0.37	-	0.10	0.03	7.82
	"	"	"	"	"	"	8-1/4	64.44	14.87	14.45	6.35	2.12	1.88	0.42	0.51	-	0.16	0.06	1.20
	"	"	"	"	"	"	EXIT	62.52	14.44	13.44	11.93	4.65	4.36	1.05	1.01	0.01	0.23	0.04	0.58
210	2.5	2.0	0.64	2000	1500	NO	EXIT	60.17	12.62	14.44	16.46	5.92	5.77	1.36	1.58	0.01	0.44	0.08	1.30
211	2.5	2.0	0.64	2000	1500	NO	4-1/8	54.77	13.45	12.53	13.61	2.50	2.14	0.53	0.51	-	0.16	0.04	7.73
	"	"	"	"	"	"	8-1/4	61.17	12.92	15.70	6.70	2.05	1.94	0.42	0.60	-	0.21	0.06	1.42
	"	"	"	"	"	"	EXIT	59.44	12.20	14.65	11.77	4.36	4.17	0.99	1.09	0.01	0.28	0.06	0.81
212	2.5	2.0	0.64	2000	1700	NO	4-1/8	58.63	11.61	15.11	10.38	2.20	2.01	0.35	0.40	-	0.20	0.06	5.16
	"	"	"	"	"	"	8-1/4	64.27	9.88	19.64	4.75	2.03	1.89	0.31	0.26	0.01	0.07	0.02	0.17
	"	"	"	"	"	"	EXIT	61.94	10.84	17.44	7.21	5.62	-	0.95	0.21	0.02	0.08	0.02	0.31
214	2.5	2.0	0.64	2000	1700	NO	4-1/8	58.69	11.58	15.13									
	"	"	"	"	"	"	8-1/4	63.90	10.53	18.96	4.99	2.11	1.99	0.33	0.27	0.01	0.07	0.05	0.16
215	3.0	2.0	0.53	2000	1700	NO	4-1/8	58.69	11.71	14.87	10.48	2.29	2.35	0.34	0.65	-	0.32	0.09	4.44
	"	"	"	"	"	"	8-1/4	64.14	10.98	18.24	4.98	2.16	2.03	0.31	0.25	0.01	0.07	0.01	0.14
	"	"	"	"	"	"	EXIT	62.51	11.14	16.67	8.76	4.16	3.67	0.67	0.08	0.01	0.04	0.01	0.12
216	2.5	2.0	0.64	2000	1700	NO	4-1/8	57.97	11.40	15.05	11.07	2.31	2.24	0.37	0.53	-	0.26	0.08	5.28
	"	"	"	"	"	"	8/1/4	63.98	10.47	18.86	4.84	2.05	1.95	0.33	0.27	0.01	0.07	0.01	0.15
	"	"	"	"	"	"	EXIT	62.28	11.23	17.37	8.74	4.22	3.52	0.71	0.13	0.01	0.04	0.01	0.10

TABLE IX (Cont'd)

TEST	$(S/C)_m$	(1) $\dot{m}_w$	(1) $\dot{m}_f$	(2) SPACE VELOCITY	(3) T_{WALL}	CARBON	(4) GAS PROBE	DRY GAS COMPOSITION, MOL %											
		LB/HR	LB/HR	HR^{-1}	°F		AT INCHES	H_2	CO_2	CO	HC_T	CH_4	C_2H_4	C_2H_6	C_3H_6	C_3H_8	C_4	C_5	C_6H_{14}
218	3.5	2.0	0.46	2000	1500	NO	4-1/8	58.02	15.43	10.42	10.85	2.23	1.79	0.44	0.37	-	0.13	0.05	5.84
	"	"	"	"	"	"	8-1/4	63.28	15.71	12.13	6.23	2.22	1.99	0.40	0.53	-	0.16	0.05	0.88
	"	"	"	"	"	"	EXIT	61.68	15.50	11.94	9.92	4.24	3.49	0.85	0.74	-	0.14	0.03	0.43
219	3.5	2.0	0.46	2000	1700	NO	4-1/8	63.47	15.91	12.20	5.56	1.58	0.74	0.13	0.30	-	0.14	0.05	2.62
	"	"	"	"	"	"	8-1/4	66.04	15.25	14.81	2.62	1.61	0.69	0.16	0.07	-	0.01	-	0.08
	"	"	"	"	"	"	EXIT	66.36	17.16	11.98	3.31	2.57	0.39	0.23	0.01	-	-	0.01	0.10
220	3.5	4.0	0.92	4000	1700	NO	4-1/8	48.74	10.94	12.06	29.88	5.00	5.86	7.32	1.13	0.24	0.50	0.13	9.70
	"	"	"	"	"	"	8-1/4	58.87	12.03	15.23	12.30	4.17	4.90	0.58	1.05	0.02	0.38	0.08	1.12
	"	"	"	"	"	"	EXIT	54.90	11.47	13.46	20.46	7.17	4.90	0.58	1.05	0.02	0.38	0.08	1.12
222	3.0	4.0	1.06	4000	1700	NO	EXIT	52.84	10.84	13.42	20.68	7.62	8.95	1.17	1.44	0.04	0.49	0.09	0.88
223	3.0	4.0	1.06	4000	1700	NO	4-1/8	43.06	12.18	12.09	19.75	3.87	4.10	0.63	0.81	0.02	0.31	0.08	9.21
	"	"	"	"	"	"	8-1/4	50.16	12.14	15.19	10.83	3.53	3.78	0.56	0.90	0.02	0.33	0.07	1.64
	"	"	"	"	"	"	EXIT	47.67	12.13	12.80	18.83	7.11	7.63	1.15	1.37	0.03	0.46	0.08	1.00
224	2.5	2.0	0.64	2000	1700	NO	4-1/8	56.38	11.41	14.73	13.43	3.03	2.89	0.47	0.63	0.01	0.29	0.09	6.02
	"	"	"	"	"	"	8/1/4	62.73	10.89	18.73	7.26	3.18	2.90	0.48	0.37	0.01	0.10	0.02	0.30
	"	"	"	"	"	"	EXIT	58.96	10.54	16.43	12.22	5.68	5.15	0.96	0.22	0.01	0.08	0.02	0.10
225	2.5	2.0	0.64	2000	1700	NO	4-1/8	56.12	11.12	14.91	13.82	3.19	3.19	0.50	0.78	0.01	0.35	0.09	5.71
	"	"	"	"	"	"	8-1/4	62.93	10.75	18.87	6.79	2.77	2.42	0.42	0.29	0.01	0.73	0.01	0.14
	"	"	"	"	"	"	EXIT	60.02	10.66	16.90	11.30	5.57	4.52	0.91	0.15	0.01	0.06	0.01	0.07
226	2.5	2.0	0.64	2000	1500	NO	4-1/8	51.27	12.58	11.94	19.92	3.75	3.48	0.76	0.95	0.01	0.36	0.09	10.52
	"	"	"	"	"	"	8-1/4	57.93	12.36	14.91	13.22	4.18	4.35	0.84	1.22	0.01	0.41	0.09	2.12
	"	"	"	"	"	"	EXIT	54.63	12.69	12.60	20.83	7.76	8.07	1.66	1.79	0.02	0.28	0.09	1.16

(1) Mass flowrates of water, fuel
(2) Space velocity based on reactants' flowrates (NTP)
(3) Nominal external wall temperature based on steam + CO_2 (no reaction) data.
(4) Gas sample probe location with reference to the top of catalyst bed (Fig. 21)

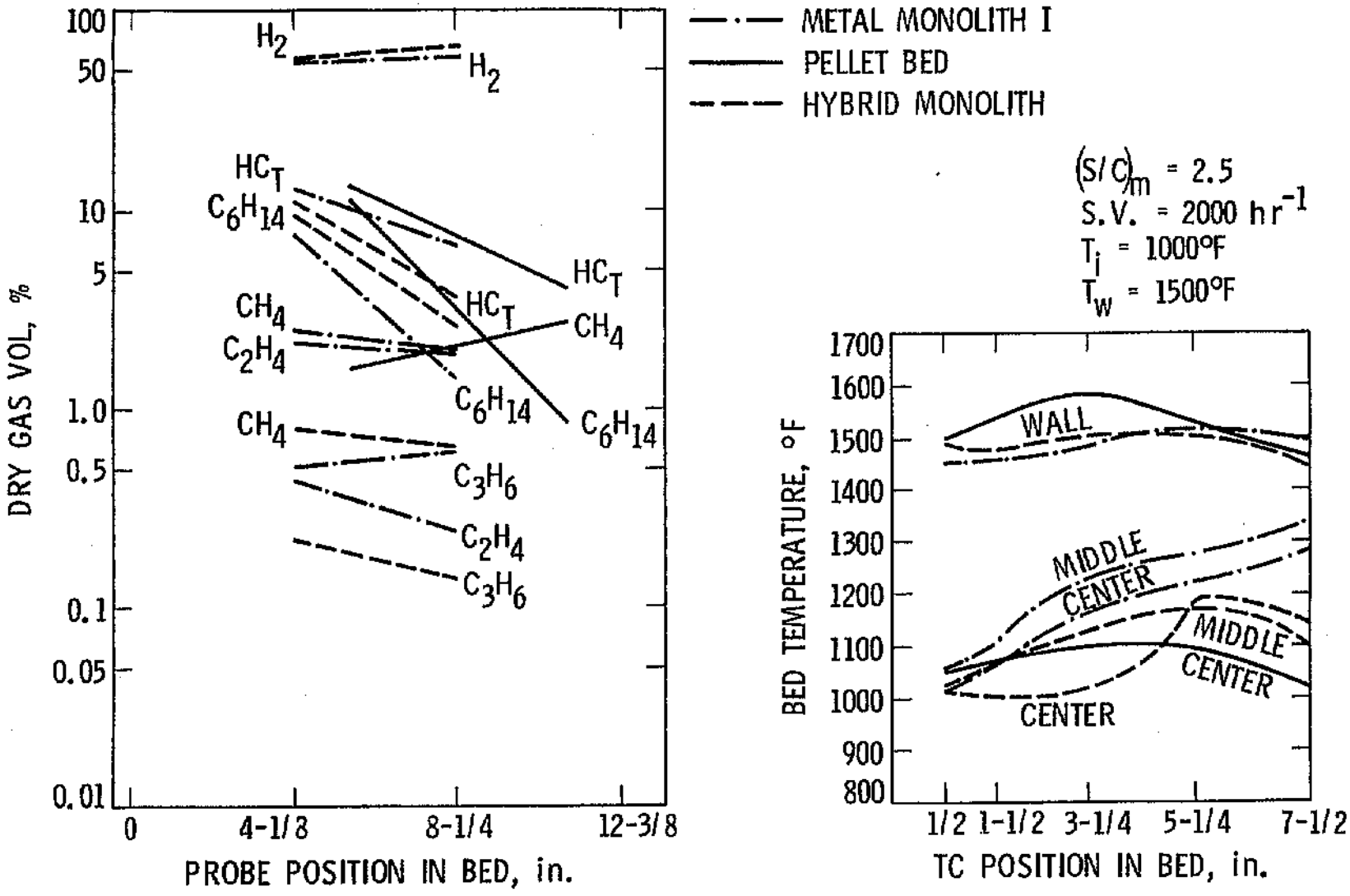

Figure 22. Steam Reforming of n-Hexane. Axial bed temperature and composition profiles for the metal monolith I, the hybrid monolith (20 in. long, ref. 11) and the G-90C pellet bed (20 in. long, ref. 11) at T_w = 1500°F.

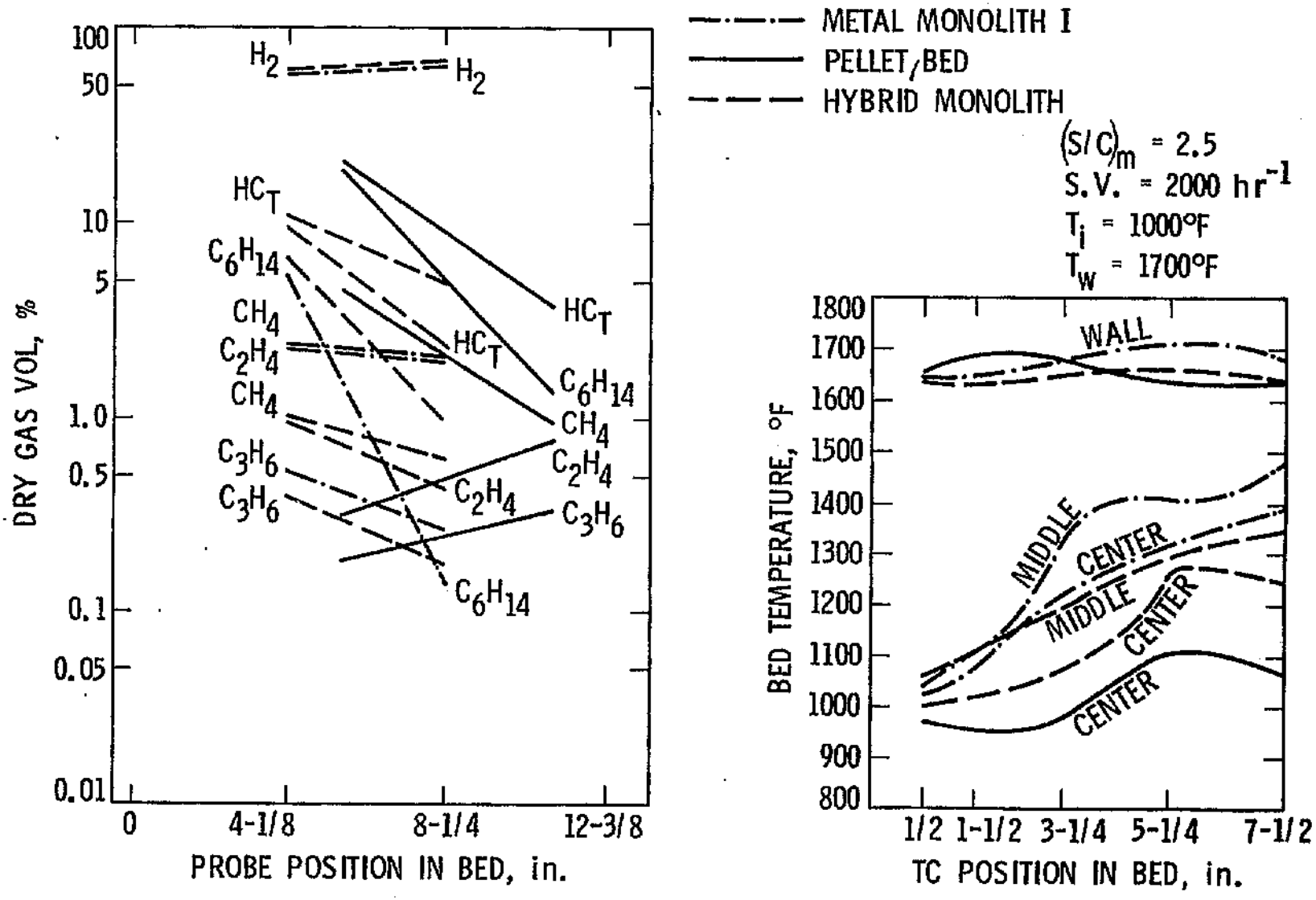

Figure 23. Steam Reforming of n-Hexane. Operating conditions are the same as in Figure 22 except that T_W = 1700°F.

Additional gas phase cracking took place downstream of the monolith catalyst in all test runs. This can be seen in Table IX from the different gas composition between gas probe 3 and product samples. This gas phase cracking is caused by the high temperatures prevailing in the lower end of the reformer, which is also inside the clam-shell furnace. Since cracking products (low molecular weight olefins) are soot precursors, carbon was expected to form and deposit on the screen and the inner tube walls close to the exit of the reactor. Indeed, upon post-inspection of the monolith and the reactor tube at the end of these tests, a large amount of flaky carbon was found at the exit of the reactor. Since the monolith cells were not plugged with carbon, these soot deposits must have been produced in the gas phase downstream of the monolith.

As can be seen from the temperature plots of Figures 22 and 23, improved radial heat transfer (from reactor wall to centerline) was observed with the 8-inch long metal monolith. For the same length of catalyst bed and same space velocities, the temperature differential from wall to centerline is minimal for the short metal monolith throughout the length of the bed. The observed temperature differences between pellet and metal monolith catalyst are easily understood. However, the difference between the metal and the hybrid monolith with identical front sections must be attributed to the lower gas flow velocity in the former rather than in the latter monolith.

Operating at higher space velocities (e.g., tests SR-219 vs. SR-220) with the short metal monolith severely limited fuel conversion to hydrogen. Higher amounts of olefinic and paraffinic intermediates were produced,

indicating that gas phase cracking reactions rather than steam reforming on the catalyst surface were more predominant in this case than at low space velocities. However, at higher space velocity, the mass diffusion limitation should be reduced, thereby enhancing surface reaction and, hence, steam reforming. If, on the other hand, the surface catalyst is not active enough, then the acidic alumina washcoat would initiate cracking, particularly when good heat transfer is possible.

In tests SR-224 (or 225) and 226, which were run at identical operating conditions as the earlier tests SR-216 and 211 respectively, a lower catalyst activity was observed by lower conversion to hydrogen and carbon monoxide. This may be due to gradual losses of washcoat (and nickel) from the monolith surface. The reactor was then opened for inspection of the catalyst. The multi-channel alumina in the conical reactor inlet was found intact, and the majority of cells in each of the four monolith segments appeared clean (open to free reactant flow). Small pieces from the center of each monolithic segment were cut for SEM examination. Cracks were found on the surface of these pieces and in several locations the washcoat was observed as islands on the bare support (Kanthal) surface. In these cases it was possible to detect the bare support by a strong signal of iron obtained by the EDAX (Energy Dispersive Analysis of X-rays) accessory of the electron microscope. Thus, the low activity observed when high space velocity operations were conducted was due to loss in catalyst activity, not reduced heat transfer.

(B) Tests With The G-90C Pellet Catalyst

Following tests with the used metal monolith, a fresh pellet catalyst bed was loaded and tested in the steam reformer. This was comprised of an 8-inch long bed of Girdler G-90C pellets (1/4 in x 1/4 in cylinders), the same catalyst as described in Table VIII. Tests were run at identical conditions as for the 8-inch long metal monolith I, keeping the inlet configuration and the thermocouple and gas probe locations the same as before (see Figure 21). Table X summarizes the data collected from tests on the pellet bed. From these and the corresponding data of Table IX for the metal monolith I, comparisons of bed temperatures and gas composition and product yields can be made between the pellet and monolithic catalysts.

Figures 24-26 show axial bed temperature profiles [centerline, middle line (half-way between centerline and the wall) and external wall temperatures] for the two catalysts under the same operating conditions. In all cases, the temperature differential between wall and either centerline or middle line was lower for the monolith in the first half of the bed. This indicates a potential improvement of the reformer performance with a monolith catalyst at the inlet where temperatures of the steam reforming catalyst are the lowest due to the endothermicity of the reaction.

The left hand side of Figures 24-26 shows dry gas analyses (as obtained by gas chromatography) for mid-bed and exit (product) gas samples. The operating conditions listed in these figures apply to both plots. Higher

TABLE X

STEAM REFORMING OF N-HEXANE ON G-90C PELLETS

TEST	$(S/C)_m$	(1) $\dot{m}_w$	(1) $\dot{m}_F$	(2) SPACE VELOCITY	(3) T_{WALL}	CARBON	(4) GAS PROBE	DRY GAS COMPOSITION, MOL %											
		LB/HR	LB/HR	HR^{-1}	°F		AT INCHES	H_2	CO_2	CO	HC_T	CH_4	C_2H_4	C_2H_6	C_3H_6	C_3H_8	C_4	C_5	C_6H_{14}
227	3.0	2.0	0.53	2000	1700	NO	4-1/8	66.84	16.24	11.15	1.87	1.84	0.01	-	-	-	-	-	0.03
	"	"	"	"	"	"	8-1/4	67.38	9.11	16.63	0.05	0.05	-	-	-	-	-	-	-
	"	"	"	"	"	"	EXIT	67.48	8.54	17.08	0.11	0.11	-	-	-	-	-	-	-
228	2.5	2.0	0.64	2000	1700	NO	4-1/8	65.76	11.63	13.59	2.51	2.21	-	-	-	-	-	-	0.30
	"	"	"	"	"	"	8-1/4	66.94	6.67	19.50	0.22	0.07	-	-	-	-	-	-	0.15
	"	"	"	"	"	"	EXIT	67.27	8.17	17.73	0.06	0.05	-	-	-	-	-	-	0.01
229	2.0	2.0	0.80	2000	1700	NO	4-1/8	63.59	11.78	13.08	5.06	2.99	0.04	0.01	0.02	-	0.01	-	1.99
	"	"	"	"	"	"	8-1/4	67.10	6.33	20.23	0.73	0.70	-	-	-	-	-	-	0.03
	"	"	"	"	"	"	EXIT	67.16	5.80	21.01	1.21	1.17	-	-	-	-	-	-	0.04
230	3.0	2.0	0.53	2000	1500	NO	4-1/8	65.54	17.47	10.37	5.25								
	"	"	"	"	"	"	8-1/4	67.48	9.77	15.40	0.29	0.12	-	-	-	-	-	-	0.17
	"	"	"	"	"	"	EXIT	67.16	8.91	16.63	0.10	0.09	-	-	-	-	-	-	0.01
231	3.0	2.0	0.53	2000	1500	NO	4-1/8	64.62	18.58	8.66	6.02	5.53	-	-	-	-	-	-	0.49
	"	"	"	"	"	"	8/1/4	67.70	11.86	14.00	0.84	0.72	-	-	-	-	-	0.01	0.11
	"	"	"	"	"	"	EXIT	68.02	11.42	14.42	0.80	0.68	-	-	-	-	-	-	0.12
232	2.5	2.0	0.64	2000	1500	NO	4-1/8	62.65	18.32	9.32	7.98	7.02	0.01	-	-	-	-	-	0.95
	"	"	"	"	"	"	8-1/4	66.40	9.93	15.76	2.50	1.96	-	-	-	-	-	-	0.54
	"	"	"	"	"	"	EXIT	66.84	9.16	16.38	0.02	-	-	-	-	-	-	-	0.02

TABLE X (Cont'd)

TEST	$(S/C)_m$	(1) $\dot{m}_w$	(1) $\dot{m}_f$	(2) SPACE VELOCITY	(3) T_{WALL}	CARBON	(4) GAS PROBE	DRY GAS COMPOSITION, MOL %											
		LB/HR	LB/HR	HR^{-1}	°F		AT INCHES	H_2	CO_2	CO	HC_T	CH_4	C_2H_4	C_2H_6	C_3H_6	C_3H_8	C_4	C_5	C_6H_{14}
233	2.0	2.0	0.80	2000	1500	NO	4-1/8	61.05	15.21	10.62	9.75	7.13	0.03	0.01	0.02	–	0.01	–	2.55
	"	"	"	"	"	"	8-1/4	63.87	10.17	15.18	6.81	6.76	0.01	–	–	–	–	0.01	0.03
	"	"	"	"	"	"	EXIT	64.62	9.18	16.11	6.16	6.09	0.02	0.01	0.01	–	–	–	0.03
234	3.5	2.0	0.46	2000	1500	NO	4-1/8	67.27	18.43	9.21	1.71	1.51	–	–	–	–	–	–	0.20
	"	"	"	"	"	"	8-1/4	67.59	14.24	12.21	0.37	0.12	–	–	–	–	–	–	0.25
	"	"	"	"	"	"	EXIT	67.70	15.17	12.33	0.42	0.24	–	–	–	–	–	0.01	0.17
235	3.5	2.0	0.46	2000	1700	NO	4-1/8	68.02	14.01	12.32	0.29	0.24	–	–	–	–	–	–	0.05
	"	"	"	"	"	"	8-1/4	68.02	10.98	14.83	0.02	0.01	–	–	–	–	–	–	0.01
	"	"	"	"	"	"	EXIT	68.35	10.40	15.34	0.02	0.01	–	–	–	–	–		0.01
236	3.0	2.0	0.53	2000	1700	NO	4-1/8	67.05	12.07	13.15	1.18	1.04	–	–	–	–	–	–	0.14
	"	"	"	"	"	"	8-1/4	67.48	8.12	16.86	0.04	0.03	–	–	–	–	–	–	0.01

(1) - (4) See Table IX

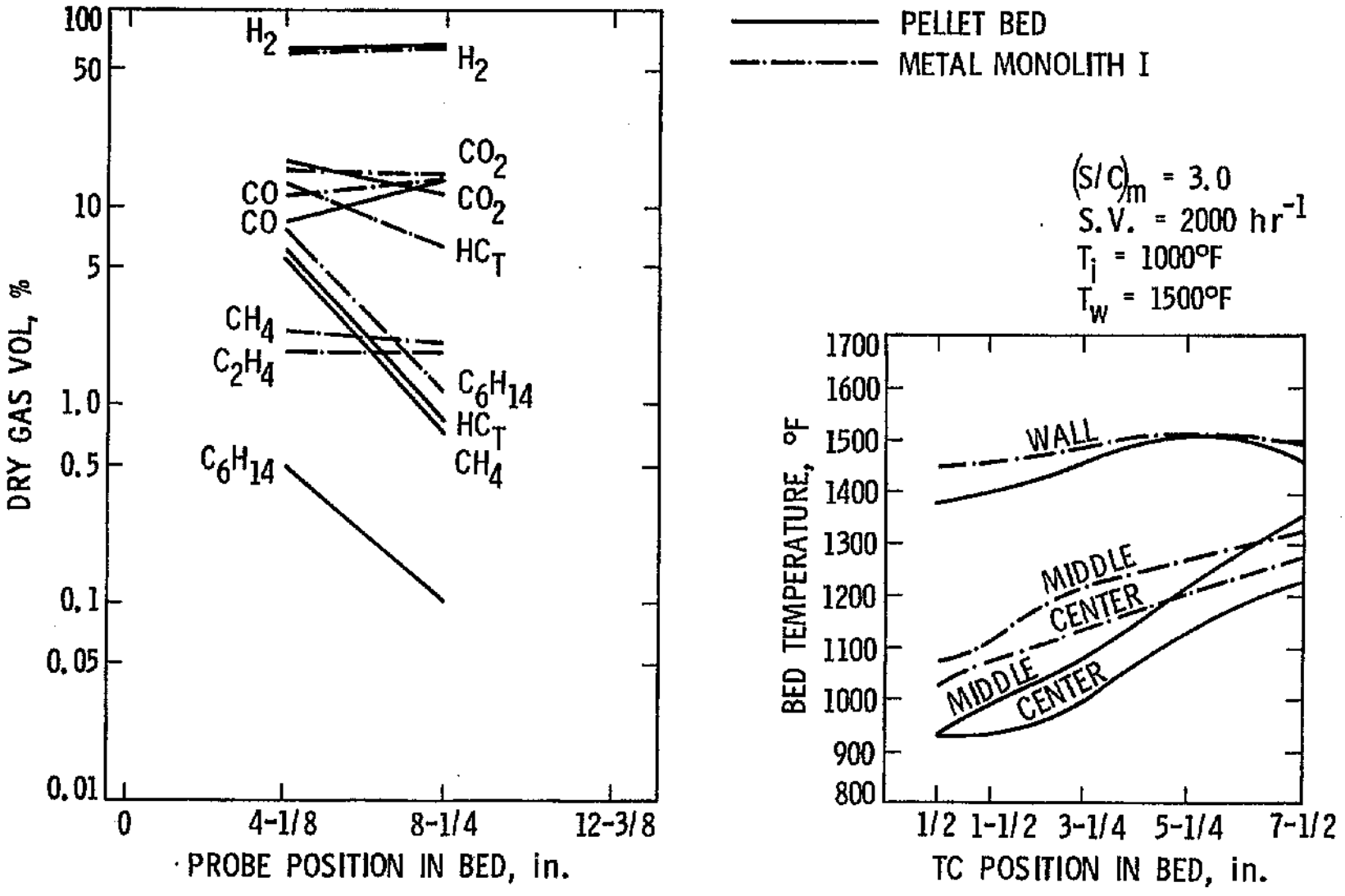

Figure 24. Steam Reforming of n-Hexane. Axial bed temperature and composition profiles for the metal monolith I and the 8-in. long G-90C pellet bed.

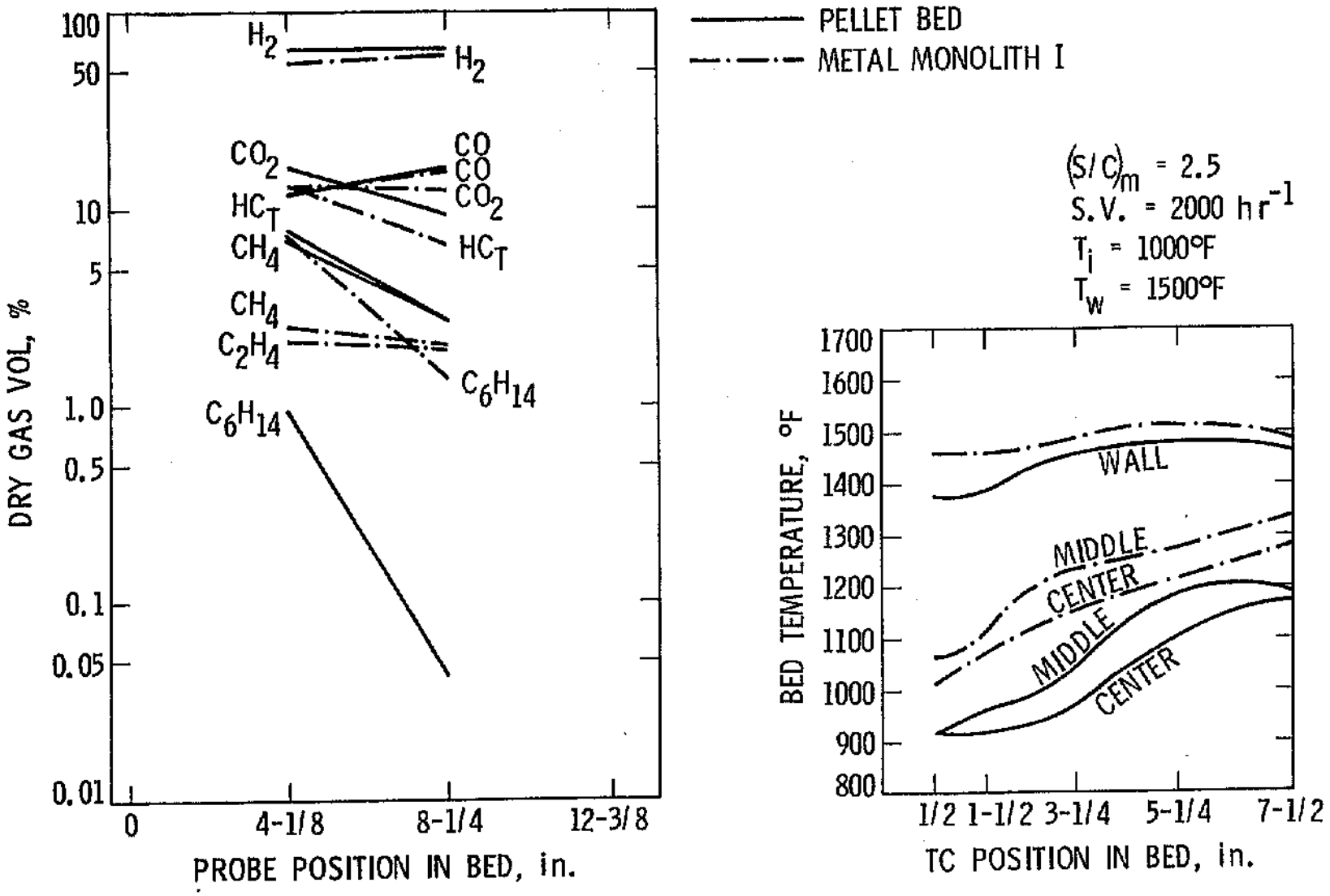

Figure 25. Steam Reforming of n-Hexane. Operating conditions are the same as in Fig. 24, except that $(S/C)_m$ = 2.5.

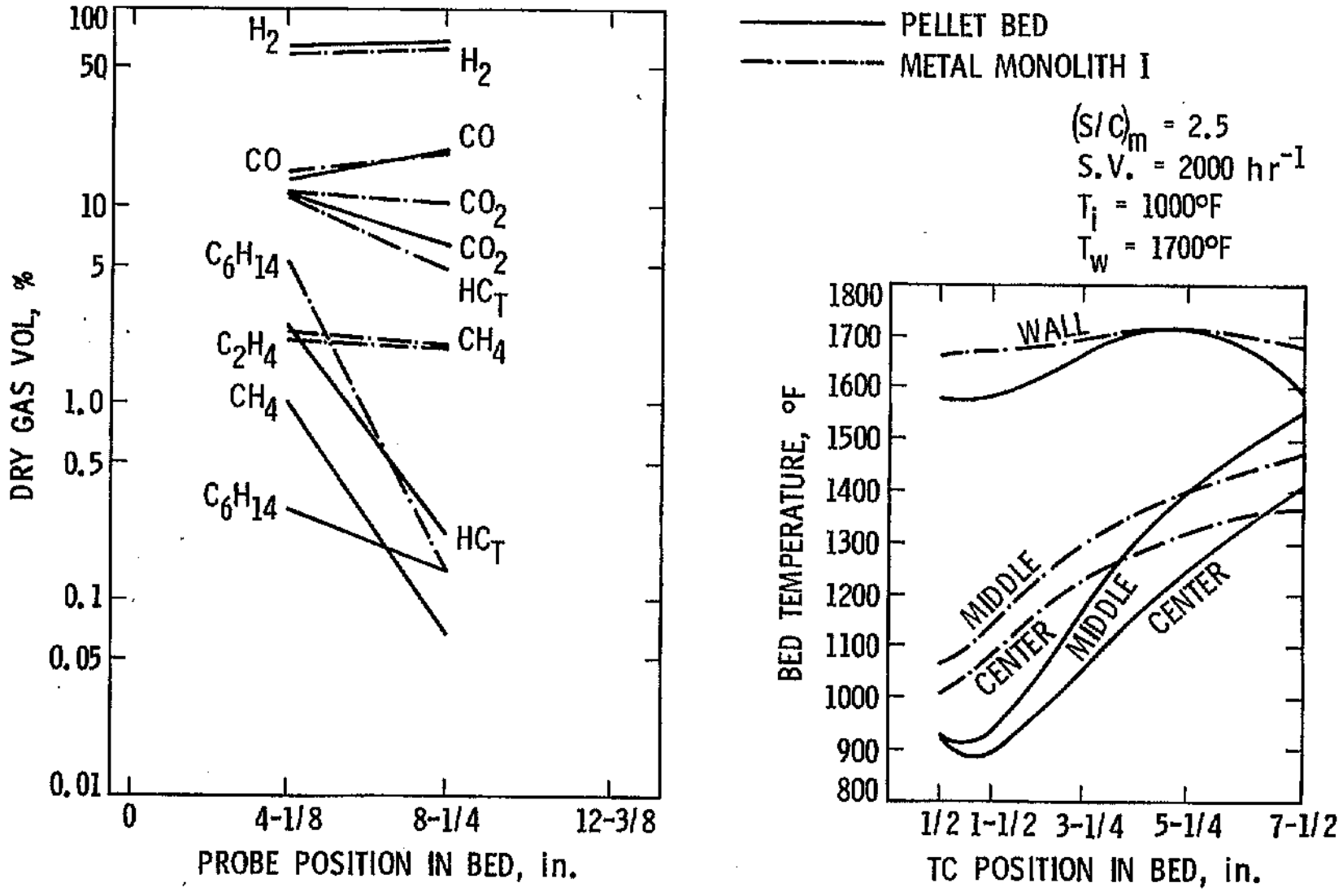

Figure 26. Steam Reforming of n-Hexane. Operating conditions are the same as in Fig. 25, except that T_W = 1700°F.

hydrogen yields were obtained and the amounts of hydrocarbon intermediates and methane at the exit of the pellet bed were extremely low.

In comparison, these results indicate that the metal monolith I had a lower overall conversion efficiency than the pellet bed of equal size. However, a one-to-one comparison between the two catalysts cannot be made, because of their non-compatible nickel loading, dispersion, and surface areas and the fluid dynamics involved. In order for identical comparisons of catalysts with respect to heat transfer, catalyst loading, surface area, gas flows and related conditions, a more detailed characterization of monolithic catalysts is necessary.

(C) Tests With The Metal Monolith II

Following the pellet tests, reactive characteristics were determined for the metal monolith II, which had been impregnated with nickel in-house to a loading higher than that of metal monolith I (Table VIII). Tests SR-280 through 294 were run with n-hexane on this new metal monolith at P = 1 atm, T_{inlet} = 1000°F, and for $(S/C)_m$ ratios of 3.5, 3.0, 2.5, 2.0, and 1.5. Reactor wall temperatures T_w of 1500°F and 1700°F, and nominal space velocities of 2000 and 4000 hr^{-1} were used. The data from tests with the metal monolith II are summarized in Table XI.

Initial tests were run at T_w = 1700°F. Improved heat transfer between reactor wall and catalyst bed was observed with the metal monolith as compared to the pellets, particularly at the top of the bed. This is

TABLE XI

STEAM REFORMING OF N-HEXANE ON THE METAL MONOLITH II

TEST SR -	$(S/C)_m$	(1) $\dot{m}_w$ LB/HR	(1) $\dot{m}_f$ LB/HR	(2) SPACE VELOCITY HR^{-1}	(3) T_{WALL} °F	CARBON	(4) GAS PROBE AT INCHES	DRY GAS COMPOSITION, MOL %											
								H_2	CO_2	CO	HC_T	CH_4	C_2H_4	C_2H_6	C_3H_6	C_3H_8	C_4	C_5	C_6H_{14}
280	3.0	2.0	0.53	2000	1700	NO	4-1/8	66.92	13.63	12.82	0.80	0.46	-	0.05	-	-	-	-	0.29
"	"	"	"	"	"	"	8-1/4	67.31	9.04	16.49	0.01	0.01	-	-	-	-	-	-	-
281	2.5	2.0	0.64	2000	1700	NO	4-1/8	66.93	9.94	15.84	0.80	0.60	0.02	0.01	0.01	-	-	-	0.17
"	"	"	"	"	"	"	8-1/4	67.46	6.29	19.67	0.05	0.03	-	-	-	-	-	-	0.02
282	2.0	2.0	0.80	2000	1700	NO	4-1/8	64.31	9.43	14.88	3.41	1.07	0.14	0.03	0.08	-	0.04	0.01	2.04
"	"	"	"	"	"	"	8-1/4	67.22	4.67	22.48	0.52	0.52	-	-	-	-	-	-	-
283	1.5	2.0	1.06	2000	1700	?	4-1/8	57.28	7.91	14.71	11.60	1.60	0.60	0.14	0.29	-	1.27	0.04	7.65
"	"	"	"	"	"	"	8-1/4	66.30	3.26	24.57	1.70	1.59	0.03	0.02	0.01	-	-	-	0.05
284	3.0	2.0	0.53	2000	1500	NO	4-1/8	65.54	16.30	10.11	2.93	0.87	0.02	0.01	0.01	-	0.01	-	2.01
"	"	"	"	"	"	"	8-1/4	67.54	10.42	15.62	0.19	0.19	-	-	-	-	-	-	-
285	2.5	2.0	0.64	2000	1500	NO	4-1/8	61.39	15.02	9.58	6.58	1.14	0.10	0.04	0.05	-	0.02	0.01	5.22
"	"	"	"	"	"	"	8-1/4	67.11	9.59	15.60	1.12	0.92	0.02	0.02	-	-	-	-	0.16
286	2.0	2.0	0.80	2000	1500	NO	4-1/8	53.88	11.51	10.81	13.03	1.84	0.83	0.34	0.27	-	0.08	0.02	9.65
"	"	"	"	"	"	"	8-1/4	62.65	9.95	15.85	3.44	1.85	0.40	0.16	0.15	-	0.04	0.01	0.85
287	1.5	2.0	1.06	2000	1500	NO	4-1/8	62.48	6.75	10.86	15.77	3.34	0.77	0.31	0.25	-	0.07	0.01	11.02
"	"	"	"	"	"	"	8-1/4	50.79	6.44	17.09	5.42	3.16	0.80	0.31	0.27	-	0.07	0.02	0.79

TABLE XI (Cont'd)

TEST SR -	$(S/C)_m$	(1) $\dot{m}_w$ LB/HR	(1) $\dot{m}_f$ LB/HR	(2) SPACE VELOCITY HR^{-1}	(3) T_{WALL} °F	CARBON	(4) GAS PROBE AT INCHES	DRY GAS COMPOSITION, MOL %											
								H_2	CO_2	CO	HC_T	CH_4	C_2H_4	C_2H_6	C_3H_6	C_3H_8	C_4	C_5	C_6H_{14}
288	3.5	2.0	0.46	2000	1500	NO	4-1/8	65.58	18.59	8.20	2.98	0.82	0.01	0.01	0.01	-	-	-	2.14
	"	"	"	"	"	"	8-1/4	67.59	17.52	10.73	0.71	0.33	-	-	-	-	-	-	0.38
289	3.0	4.0	1.06	4000	1500	NO	4-1/8	52.53	15.96	7.35	14.63	1.79	1.30	0.35	0.33	-	0.09	0.01	10.76
	"	"	"	"	"	"	8-1/4	60.96	15.36	10.46	6.02	1.67	1.22	0.31	0.33	-	0.28	0.02	2.19
290	3.5	4.0	0.92	4000	1500	NO	4-1/8	58.42	15.98	8.72	8.34	0.83	0.46	0.14	0.12	-	0.04	0.01	6.74
	"	"	"	"	"	"	8-1/4	65.21	14.97	12.83	1.97	0.72	0.35	0.10	0.09	-	0.05	0.01	0.67
291	3.5	4.0	0.92	4000	1700	NO	4-1/8	59.37	15.07	9.50	7.06	0.65	0.22	0.05	0.07	-	0.04	0.01	6.02
	"	"	"	"	"	"	8-1/4	66.07	11.66	14.24	1.10	0.54	0.16	0.04	0.03	-	0.01	-	0.32
292	3.0	4.0	1.06	4000	1700	NO	4-1/8	57.91	14.06	9.02	14.03	1.03	0.13	-	0.16	-	0.08	0.03	12.60
	"	"	"	"	"	"	8-1/4	65.32	11.42	14.17	1.83	0.85	0.34	0.09	0.05	-	0.02	0.01	0.48
293	3.0	2.0	0.53	2000	1700	NO	4-1/8	65.95	13.33	12.41	2.24	0.57	0.08	0.02	0.04	-	0.02	0.01	1.11
	"	"	"	"	"	"	8-1/4	67.38	9.60	16.11	0.32	0.31	-	-	-	-	-	-	0.01
294	2.5	2.0	0.64	2000	1700	NO	4-1/8	63.74	11.68	12.88	3.79	0.86	0.23	0.04	0.11	-	0.06	0.02	2.47
	"	"	"	"	"	"	8-1/4	66.90	6.91	19.71	0.46	0.43	0.01	0.01	-	-	-	-	0.01

(1) - (4) See Table IX

shown by the axial bed temperature profiles plotted in Figures 27 and 28 for the metal monolith II and pellets at T_w = 1700°F, S.V. = 2000 hr^{-1}, and $(S/C)_m$ = 2.5 and 2.0, respectively. Axial bed composition profiles for the same operating conditions are also shown in Figures 27 and 28. Higher conversion of hexane to hydrogen and carbon monoxide was attained with the monolith, and the amounts of methane and unconverted hexane were lower than for the pellets throughout the bed and at the exit. Thus, this monolith bed appears to have a higher steam reforming activity than the pellets, even though the actual space velocity is approximately twice as high for the monolith (void fraction ~ 70%) as for the pellets (void fraction ~ 30%). This activity difference could also be due in part to the higher nickel loading and perhaps the nickel dispersion, because of the high surface alumina washcoat of the metal monolith.

In test SR-283 with $(S/C)_m$ = 1.5, carbon might have been formed in the upper half of the monolith. This was indicated by a gradual decline in activity observed in following tests, but could not be confirmed at that point because there was no rise in the pressure drop through the bed, and no carbon fines were found in the gas samples. Figure 29 shows axial temperature and composition profiles for T_w = 1500°F, $(S/C)_m$ = 3.0, and S.V. = 2000 hr^{-1} (test SR-284). The monolith still has a better conversion efficiency than the pellets, but, as can be seen from the hexane profile, the unconverted hexane coming out of the upper two monolith segments is higher than that corresponding to the same location in the pellet bed.

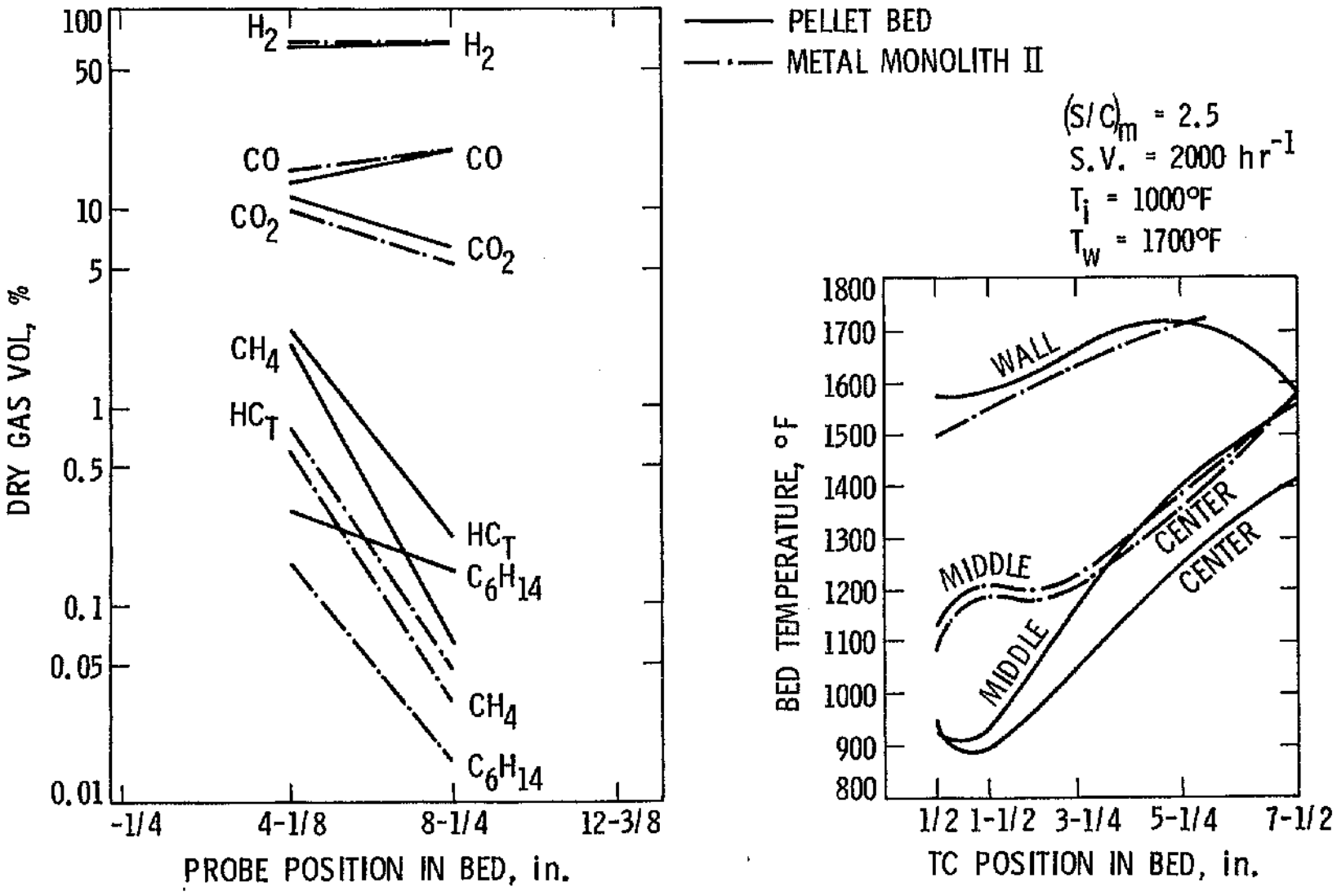

Figure 27. Steam Reforming of n-Hexane. Axial bed temperature and composition profiles for the metal monolith II and G-90C pellets at T_W = 1700°F, S.V. = 2000 hr^{-1}, and $(S/C)_m$ = 2.5.

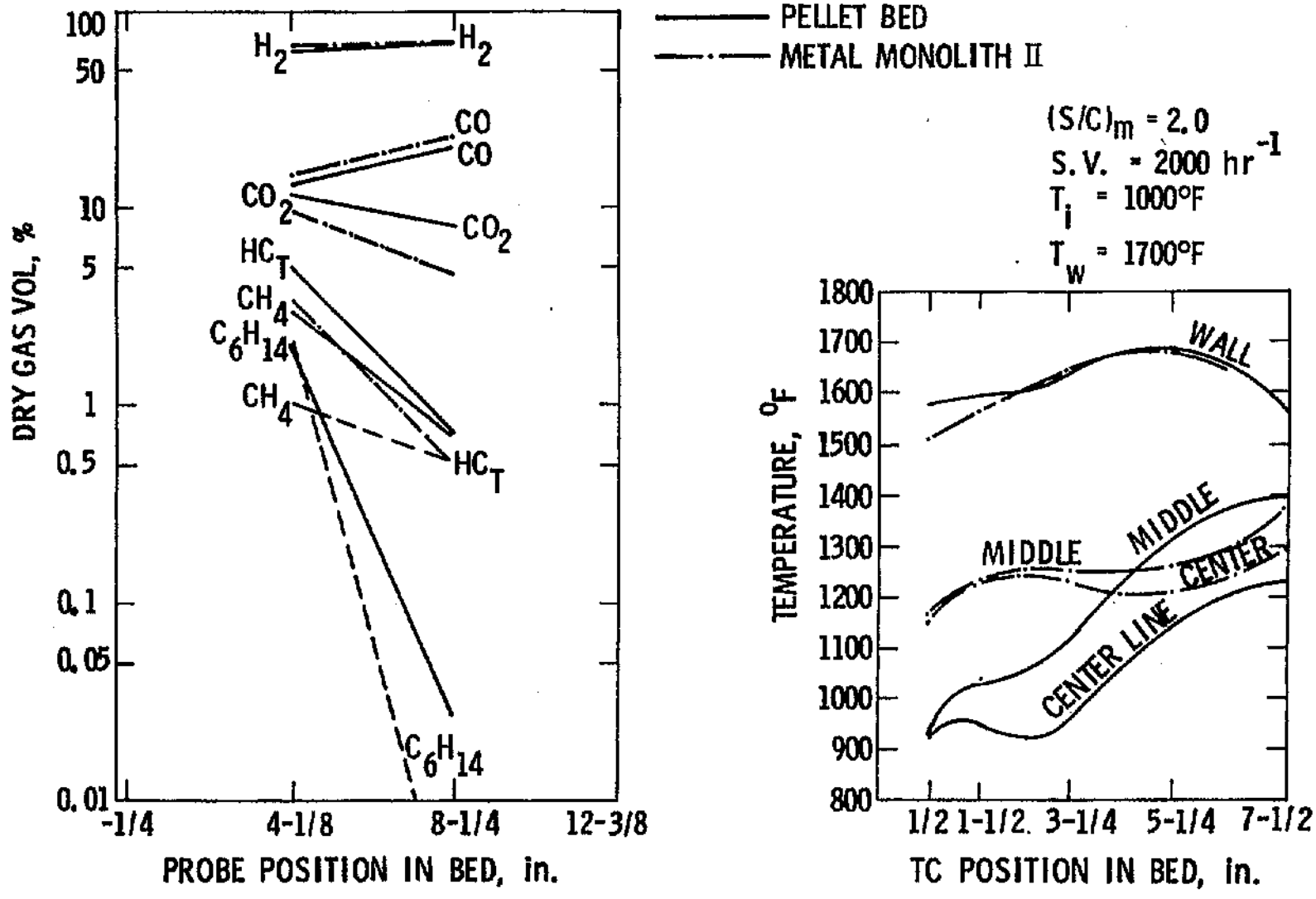

Figure 28. Steam Reforming of n-Hexane. Operating conditions are the same as in Fig. 27, except that $(S/C)_m$ = 2.0.

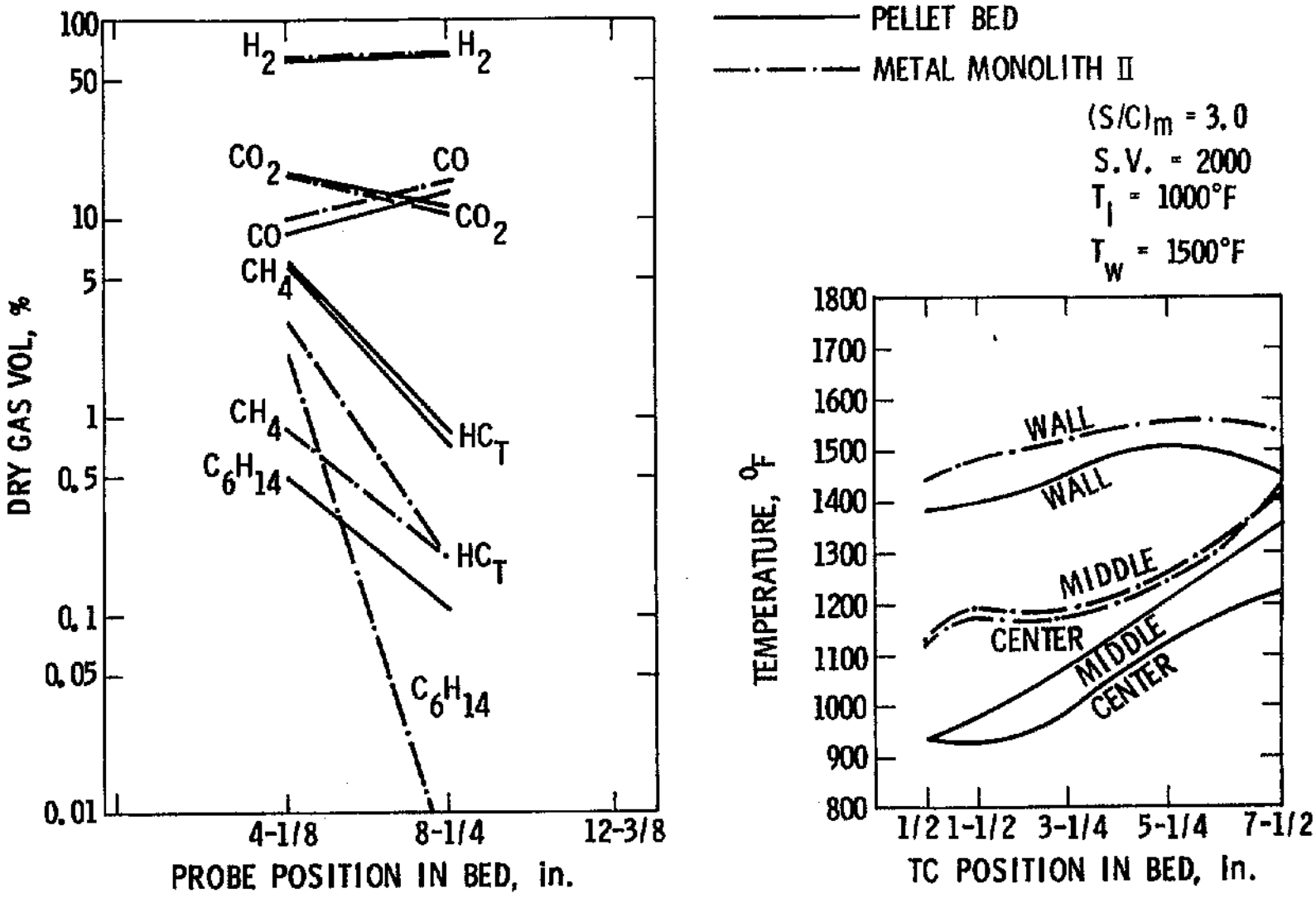

Figure 29. Steam Reforming of n-Hexane. Axial bed temperature and composition profiles for the metal monolith II and G-90C pellets after carbon formation had taken place in the monolith (test SR-284).

Starting with test SR-285, the decline in monolith steam reforming activity became evident. Figure 30 depicts this for the conditions of test SR-286. Higher amounts of unconverted hexane throughout the bed are now observed for the monolith, and olefins (ethylene, propylene) appear in the bed, indicating high gas phase cracking rates. The amount of methane, however, is much lower for the monolith than for the pellets, so that the percentage of total hydrocarbons at the monolith exit is lower. Radial heat transfer rates for the monolith have remained higher at these conditions, and continued to do so in all subsequent tests.

The effects of $(S/C)_m$ ratios and space velocity changes on the monolith performance were similar to those for the G-90C pellet bed. Thus, at higher $(S/C)_m$ ratios, the hexane conversion was higher, and lower methane was produced throughout the bed. Higher space velocities, resulted in lower catalyst temperatures and lower conversion efficiency as can be seen from the data of Table XI. Figure 31 compares the performance of metal monolith II to the pellet bed for a space velocity of 4000 hr^{-1}. The comparative heat transfer characteristics and steam reforming activity of each of these two catalysts follows the same trend as in the case of lower space velocities.

Tests SR-293 and 294 were run at identical conditions as the first tests of the series, SR-280 and 281, respectively, to determine the effect of the presumed carbon deposits in the bed on the monolith activity. Figure 32 shows axial bed temperature and composition profiles for the conditions of tests SR-281 and 294, run with the metal monolith before and (presumably) after carbon formation had taken place. Lower bed tempera-

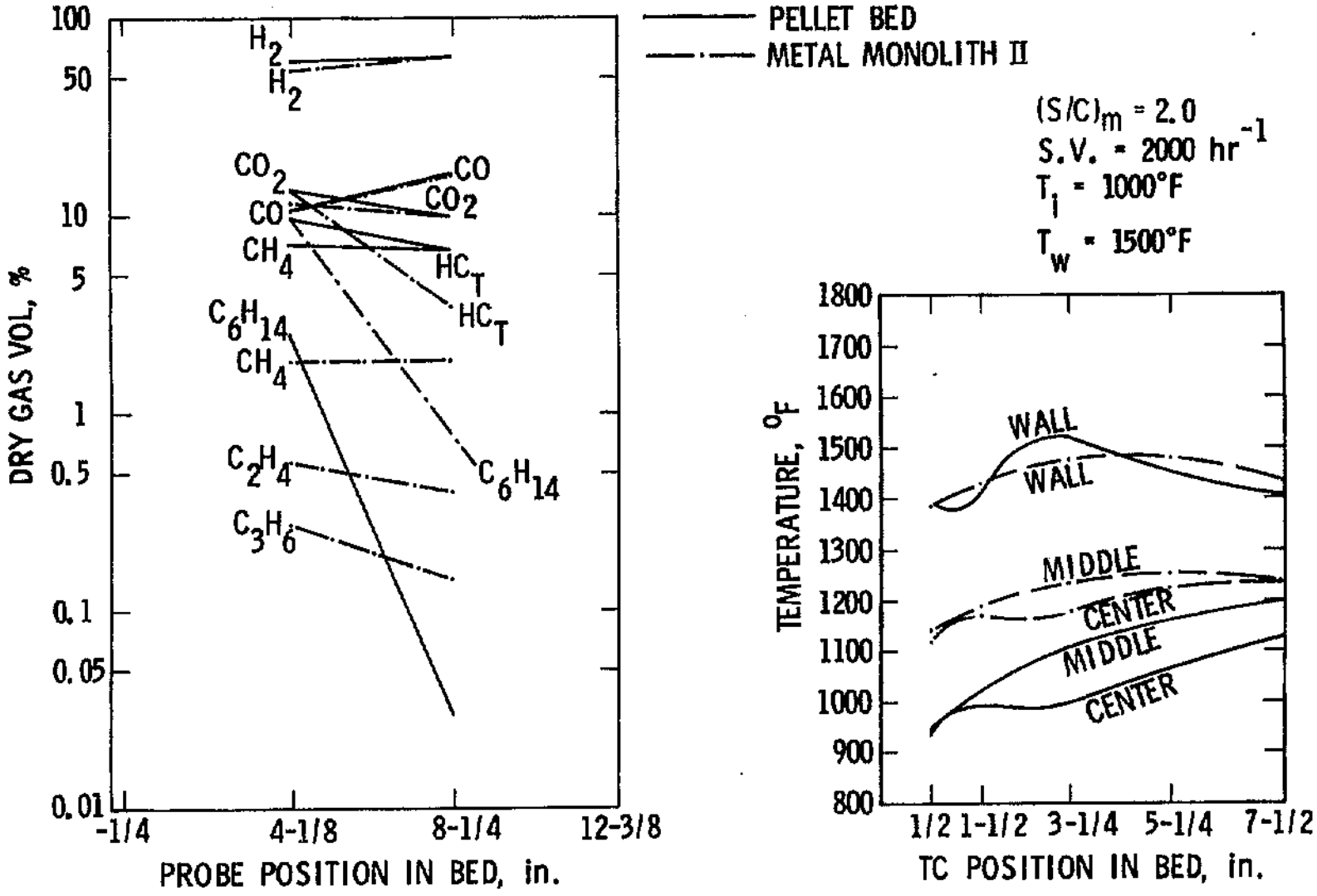

Figure 30. Steam Reforming of n-Hexane. The metal monolith II data (test SR-286), indicate a further decline in monolith activity due to carbon plugging of monolith cells.

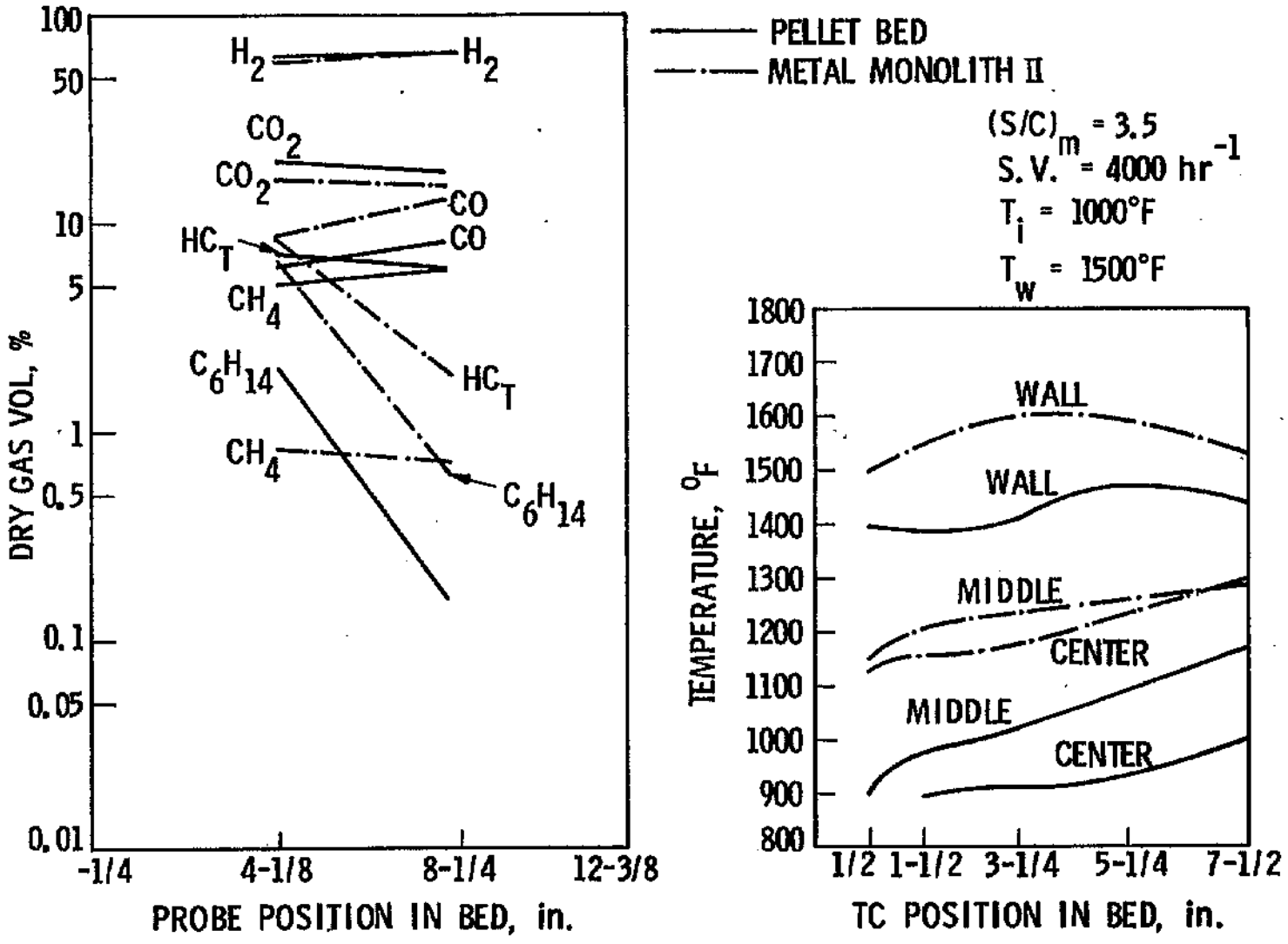

Figure 31. Steam Reforming of n-Hexane. Axial bed temperature and composition profiles for the metal monolith II and the G-90C pellets at the higher space velocity of 4000 hr^{-1}.

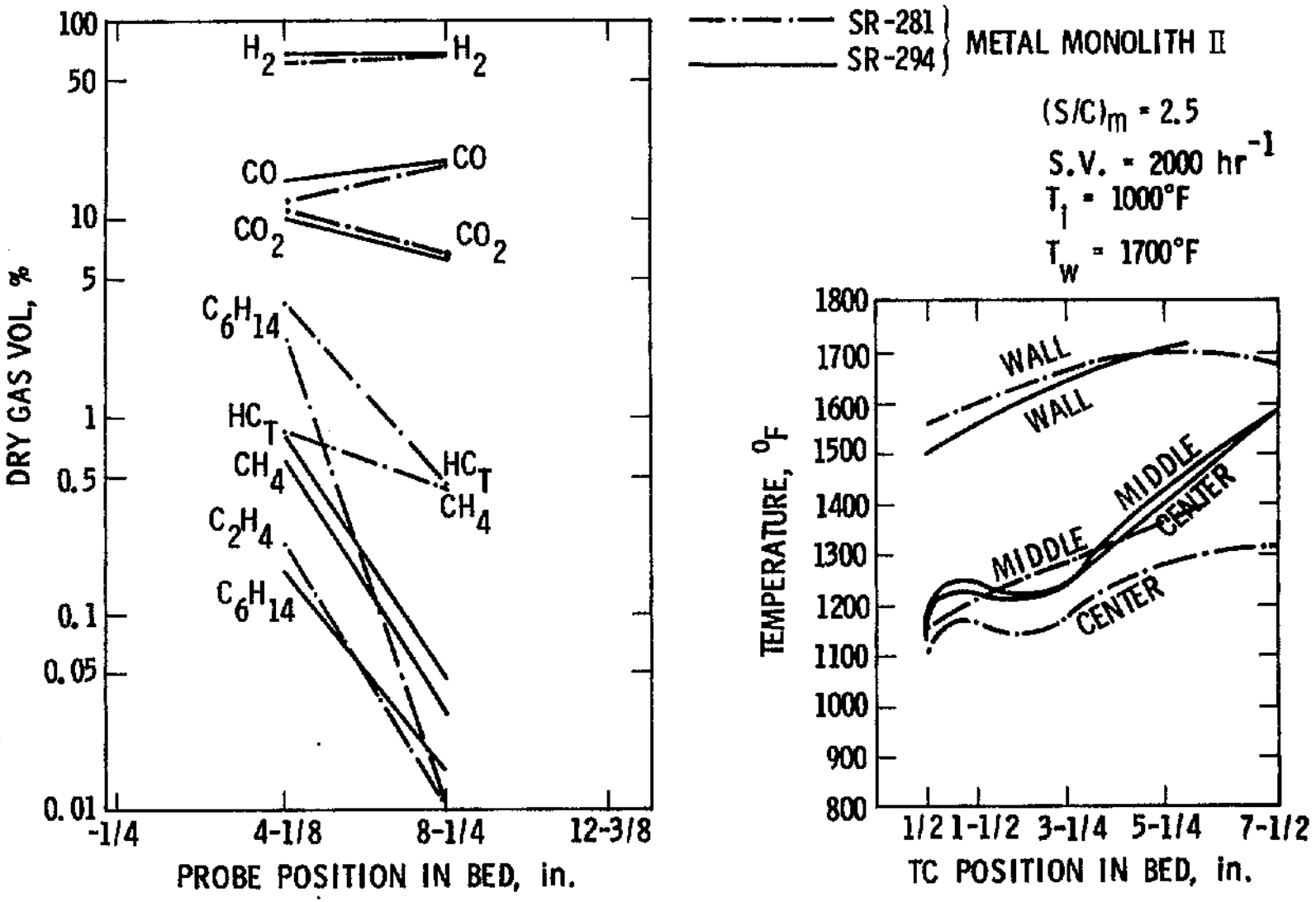

Figure 32. Steam Reforming of n-Hexane. Performance comparison of the metal monolith II before (test SR-281) and after (test SR-294) carbon formation in the bed.

tures were observed for the SR-294 test, which may be attributed to partial carbon plugging of monolithic cells. This would force all gas flow through fewer cells, i.e., a lower volume of the catalyst would be used for reaction, space velocity would be higher, and temperatures lower. For the same reason, more gas phase reactions (cracking) would take place, and the monolith would have a lower conversion efficiency. This is shown in the composition profiles of Figure 32. Ethylene is observed only for test SR-294, in which the methane content is also higher, while lower amounts of hydrogen and carbon monoxide are produced. Unconverted hexane coming out of the second monolith segment is much higher than before, but this rapidly decreases in the lower part of the bed, where initial activity appears to be retained.

Post-inspection of the monolith after test SR-294 verified the existence of carbon deposits in the upper half of the bed only, in agreement with indications from the experimental data discussed above. Figure 33 shows pictures (front and bottom view) of the four monolithic segments after they were taken out of the reactor. The third and fourth monoliths were clean throughout, except that black chunks of carbon were deposited on the top of the third monolith. This carbon had presumably been formed in the gas phase in this region (void) where the thin Inconel spacer allows for gas mixing. The bottom of the fourth segment was clean, but as the pieces were being pushed upwards to take them out of the reactor tube, some soft carbon was filtered to the bottom, leaving the imprint shown in Figure 33.

(a)

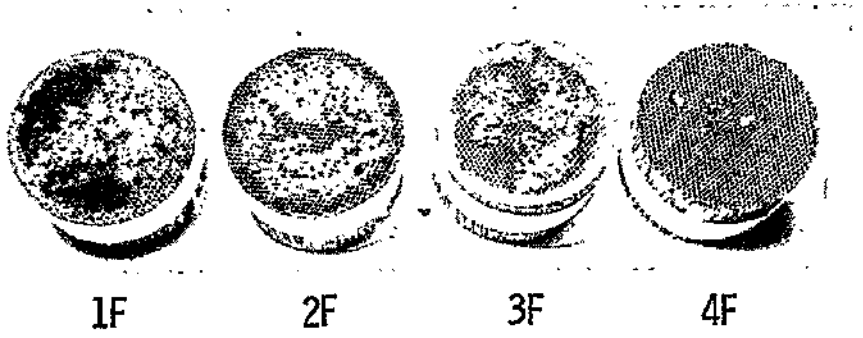

(b)

Figure 33. Pictures of the four metal monolith segments as retrieved after test SR-294 showing carbon deposition patterns. (a) Front view, (b) Bottom view.

The bottom of the cells just above the spacer between the second and third monoliths was filled with soft grey carbon fines to 1/4 in., while the top of the second monolith was partially plugged with hard black carbon. This carbon had a chunky appearance and was found to extend down inside the cells to 1/8 in. Catalyst samples from the top of the second monolith were examined by SEM. As shown in the photomicrograph of Figure 34, some of the observed carbon was surface grown (whisker growths on the surface). This presents evidence of gas/surface interaction, i.e., carbon was not formed in the gas phase (homogeneous) only. The top area of the first monolith segment was nearly all plugged with very hard black carbon. (Most of the cells that were open were found around the outer edges of the monolith.) This carbon must have originated from gas phase reactions upstream of the monolith, because carbon chunks mixed with the multi-channel alumina were also found in the conically shaped inlet. Since the inlet temperature (1000°F) is not high enough for extensive hexane thermocracking to take place, it appears that non-uniform flow and mixing conditions might have existed in the inlet region which enhanced the coking rate of hexane. To prevent this, the inlet design of the reformer may be modified to decrease the void and improve the mixing and flow distribution of the reactants.

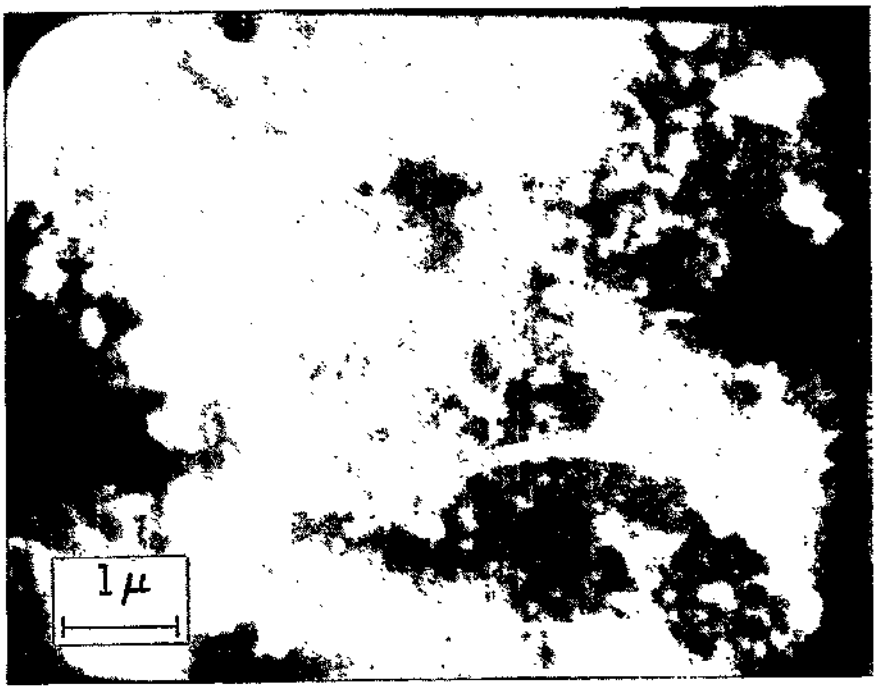

Figure 34. SEM photomicrograph of the top surface of the second piece of metal monolith II showing surface grown carbon (whisker growths).

SUMMARY

Steam reforming of hydrocarbons is an endothermic reaction whose thermal and conversion efficiencies are limited by heat transfer from the reactor wall into and throughout the catalyst bed. The heat transfer limitation is believed to be due, in part, to conduction which is affected by edge and point contact of the catalyst in a typical packed bed and also by the insulating property of the catalyst support material. Catalyst geometry is normally that of pellets or Raschig rings with dimensions compatible with a given reactor size (diameter, length) to provide optimal void-to-catalyst surface ratio. Optimization of this ratio, for the flows used, leads to control of gas phase and surface reactions and heat transfer via convection and conduction during tortuous path flow through the packed bed.

Heat conductivity improvements by ceramic monolithic supported catalysts in combustion and methanation reactions have been demonstrated. In these exothermic reactions, heat is conducted out more efficiently by monoliths than by packed beds. Application of these types of catalysts to steam reforming, therefore, appeared to be advantageous for transferring heat in the opposite direction, i.e., into the catalyst bed. The initial purpose for the experimental steam reforming work conducted in this contract was to examine the effect of this novel approach to transferring heat into the catalyst bed.

With catalyst supports that have a honeycomb structure, heat transfer by conduction directly from the walls through the bed is possible. The restriction due to edge and point contact is removed. Monolith support material may be ceramic, which is relatively inexpensive yet insulating in nature, as compared

to a metal support. The contact between a monolithic support and the reactor wall can not be direct when the monolith material is ceramic but can be direct when the material is metal. In both cases, however, uniformity throughout the catalyst bed is maintained via the integral support configuration.

A further consideration in comparing a honeycomb structure monolith to pellets is in regard to the flow pattern. Passage of gases through the pellets results in a tortuous multi-directional flow, with a typical 30% void fraction within a given reactor bed volume. Flow through a honeycomb monolith catalyst, on the other hand, is a stream line flow, each channel serving as a "mini-reactor tube". The availability of catalyst surface is, therefore, different in these two catalyst bed geometries.

The catalyst support used in the initial tests was ceramic (Cordierite) possessing a coating of γ-alumina. This "washcoat" provided a surface with uniform porosity and high area onto which the catalyst was supported. Nickel catalyst on this support was found not to be an acceptable catalyst system because of high carbon production and subsequent erosion of ceramic support, particularly at the inlet section. The silica content of the Cordierite may also have contributed to the structural deterioration by hydrothermal leaching. When heat transfer through the bed is high and the activity or availability of the catalyst is low, gas phase as well as surface carbon formation could readily take place when the void-to-surface ratio is high. The specific cause of carbon formation was not ascertained in the ceramic tests.

The key experiments during this work were directed toward determining the relationships between (1) location of carbon formation within the catalyst bed

and ceramic support deterioration, (2) metal monolith and pellet performance, and (3) catalyst loadings on metal monoliths.

In order to define whether the inlet area of the catalyst bed was responsible for the previously observed destruction of the Cordierite-supported nickel catalyst, the inlet section was replaced with metal-supported nickel catalyst. The nickel loading and void fraction (~70%) were nearly the same. Results indicated that Cordierite honeycomb monoliths were not suitable for steam reforming under the conditions tested, as evidenced by their observed deterioration when located in the bottom half of the reactor. Changes in nickel loading (activity), cell density (void fraction), and washcoat acidity may have altered this condition, but these parameters were not investigated.

Performances of metal monoliths with two different loadings of nickel were compared to pellets. Temperature and product profiles of metal monoliths with two different catalyst loadings were necessary to determine whether catalyst loading (surface reaction) or void fraction (gas phase reaction) was responsible for conversion.

The conclusions based on comparing data, Table XII, from the two metal monolith catalysts are (1) higher catalyst loading increases conversion, (2) lower catalyst loading increases methane production, and (3) changes in temperature and $(S/C)_m$ ratio are reflected in conversion more apparently in the higher loaded catalyst. Since no carbon formed at $(S/C)_m > 2.0$, even when high temperatures were maintained due to high heat transfer (and low conversion in the case of the low activity catalyst), it appears that gas phase carbon formation is not the major contributor to carbon formation in the Cordierite and hybrid bed

TABLE XII

GAS COMPOSITION COMPARISONS FROM STEAM REFORMING
OF N-HEXANE ON PELLETS AND TWO METAL MONOLITHS

$(S/C)_m$ = 2.5, S.V. = 2000 hr^{-1} T_i = 1000°F							
Gas Species	Gas Probe	Pellets		Metal Monolith I		Metal Monolith II	
		T_w=1500°F	1700°F	1500°F	1700°F	1500°F	1700°F
CH_4	#2	7.02	2.21	2.50	2.20	1.14	0.60
	#3	2.78	0.07	2.05	2.03	0.92	0.03
C_6H_{14}	#2	0.95	0.30	7.73	5.16	5.22	0.17
	#3	0.42	0.15	1.42	0.17	0.16	0.02
$(S/C)_m$ = 3.0, S.V. = 2000 hr^{-1} T_i = 1000°F							
Gas Species	Gas Probe	Pellets		Metal Monolith I		Metal Monolith II	
		T_w=1500°F	1700°F	1500°F	1700°F	1500°F	1700°F
CH_4	#2	5.53	1.84	2.34	2.29	0.87	0.46
	#3	0.72	0.05	2.12	2.16	0.19	0.01
C_6H_{14}	#2	0.49	0.03	7.82	4.44	2.01	0.29
	#3	0.11	-	1.20	0.14	-	-

under similar conditions.

The heat transfer improvement in metal monoliths over pellets can specifically be attributed to the metal monolith support when the relative conversions, at constant wall temperatures, of metal monolith II and pellets are compared, Table XII. Under the same S/C, S.V. and T_i conditions, the higher catalyst loaded monolith can be seen to provide higher conversion than pellets. The comparison of their respective product and thermal profiles, Figures 27 and 29, illustrates that bed temperatures remain higher in the early section of the metal monolith bed while also maintaining higher activity than the pelleted catalyst. Thus, enhancement of heat transfer with the metal monolithic support has been demonstrated. However, information regarding the role of fluid dynamics, availability of catalyst to reactants, and void fraction is still inadequate and must be obtained to completely define the range of advantages offered by metal monolithic supported catalysts to steam reforming.

REFERENCES

1. Houseman, J. and Cerini, D.J., "On-board Hydrogen Generator for Automobiles", 11th IECEC Paper 769001, 1976.

2. Houseman, J., "Autothermal and Steam Reforming of Distillate Fuel Oils", National Fuel Cell Seminar, San Francisco, California, July 1978.

3. Bett, J.A.S., Lesieur, R.R., McVay, D.R. and Setzer, H.J., "Adiabatic Reforming of Distillate Fuels", ibid.

4. Gordon, S. and McBride, B.J., "Computer Program for Calculation of Complex Chemicals Equilibrium Compositions, Rocket Performance, Incident and Reflected Shocks and Chapman-Jouguet Detonations", NASA 1971.

5. Jellinek, K. and Zakowski, J., Z. Anorg. Chem. 142, 1 (1925).

6. Shah, R., Voecks, G.E. and Houseman, J., "Autothermal Reforming of No. 2 Fuel Oil", Final Report to EPRI, RP 1041-2, July 1979.

7. Bett, J.A.S., Bushnell, C.L., Buswell, R.F., Gruver, G.A., King J.M. and Kunz, H.R., "Advanced Technology Fuel Cell Program", Annual Report to EPRI, EM-1328, January 1980.

8. Houghtby, W.E., Buswell, R.F., Bett, J.A.S., Lesieur, R.R., Meyer, A.P., Preston, J.L. and Setzer, H.J., "Development of the Adiabatic Reformer to Process No. 2 Fuel Oil and Coal-Derived Liquid Fuels", Interim Report to EPRI, EM-1701, February 1981.

9. Hwang, H.S., Yarrington, R.M. and Kaufman, A., "Hydrogen Production from No. 2 Fuel Oil by Autothermal Reforming", Seventh Steam Reforming Working Group Meeting, Engelhard Industries, Menlo Park, N.J., November 1981.

10. Flytzani-Stephanopoulos, M. and Voecks, G.E., "Autothermal Reforming of n-Hexane, Benzene and n-Tetradecane", Final Report to DOE, ET-78-A-03-2042, October 1979.

11. Flytzani-Stephanopoulos, M. and Voecks, G.E., "Autothermal Reforming of n-Tetradecane and Benzene Solutions of Naphthalene on Pellet Catalysts, and Steam Reforming of n-Hexane on Pellet and Monolithic Catalyst Beds", Final Report to DOE, DE-AI03-78ET-11326, October 1980 (in press).

12. Flytzani-Stephanopoulos, M. and Voecks, G.E., "Catalytic Autothermal Reforming Increases Fuel Cell Flexibility", Energy Progress 1, 52 (1981).

13. ICI Catalysts Information Bulletin, ICI Ltd., Agricultural Division, Billingham, Cleveland, England.

14. Rostrup-Nielsen, J.R., in "Steam Reforming Catalysts. An Investigation of Catalysts for Tubular Steam Reforming of Hydrocarbons", Teknisk Forlag A-3, Copenhagen, 1975.

15. Maat, H., "The Sulfur Problem: HDS of Heavy Feed to Low S Levels", Fuel Processing for Fuel Cell Power Generation Meeting, Palo Alto, California, April 1977.